This article has been accepted for publication in a future issue of this journal, but has not been fully edited. Content may change prior to final publication. Citation information: DOI 10.1109/TSP.2021.3093260, IEEE Transactions on Signal Processing

Spatial-Slepian Transform on the Sphere

Adeem Aslam, *Student Member, IEEE*, and Zubair Khalid, *Senior Member, IEEE*

***Abstract*—We present spatial-Slepian transform (SST) for the joint spatial-Slepian domain representation of signals on the sphere to support localized signal analysis. We employ well-optimally concentrated Slepian functions, which are obtained as a solution of the Slepian spatial-spectral concentration problem of finding bandlimited and spatially optimally concentrated functions on the sphere, to formulate the proposed transform. Due to optimal energy concentration of Slepian functions in the spatial domain, the proposed spatial-Slepian transform allows us to probe spatially localized content of the signal. Furthermore, we present an inverse transform to recover the signal from its spatial-Slepian coefficients, formulate an algorithm for fast computation of SST, and carry out computational complexity analysis. We compute the spatial variance of spatial-Slepian coefficients and conduct experiments to show that spatial-Slepian coefficients have better spatial localization than scale-discretized wavelet coefficients. We present the formulation of SST for zonal Slepian functions, which are spatially optimally concentrated in the axisymmetric polar cap region, and provide an illustration using a bandlimited Earth topography map. To demonstrate the utility of the proposed transform, we carry out localized variation analysis, in which we employ SST to detect hidden localized variations in the signal. We illustrate, through a toy example, that spatial-Slepian transform yields a much better estimate of the underlying region of hidden localized variations than scale-discretized wavelet transform.**

***Index Terms*—2-sphere, spherical harmonics, Slepian spatial-spectral concentration, localized signal analysis, bandlimited signals.**

I. Introduction

Spherical signal processing is the study and analysis of spherical signals, i.e., signals which are defined on the sphere. These signals are naturally encountered in many areas of science and engineering such as computer graphics [1], medical imaging [2]–[4], acoustics [5], [6], planetary sciences [7]–[11], geophysics [12], [13], cosmology [14]–[16], quantum mechanics [17], wireless communication [18]–[20] and antenna design [21]. A natural choice of basis functions for the representation of signals on the sphere is the spherical harmonic functions (or spherical harmonics for short). Such a representation is enabled by the spherical harmonic transform (SHT) and is called the spherical harmonic (or spectral) domain representation.

The representation of a signal in the spectral domain reveals global characteristics of the signal, without any regard to the scale or localization of those characteristics. In order to probe signals at different scales, more sophisticated methods have been proposed in the literature. One such tool that has been extensively used to represent time domain signals at different scales is the wavelet transform [22]–[24], which has also been extended for signal analysis on the sphere [25]–[30]. The framework of wavelet transform uses wavelet functions to record scale-dependent information of the underlying signal as wavelet coefficients. Although wavelet functions have been shown to exhibit good spatial localization [30], they cannot be adapted to the shape of the region of interest on the sphere. Consequently, for applications where signals are to be analyzed locally over given regions on the sphere, it is imperative to find alternate methods that can be used to probe local characteristics of signals over a subset of the sphere.

Motivated by the idea of wavelet transform, which essentially spreads out the signal content in the joint space-scale domain, we seek to find a representation of signals to analyze their local characteristics in an effort to detect localized hidden features. Naturally, we revert to Slepian spatial-spectral concentration problem on the sphere [31]–[36], which results in optimally localized basis functions, called Slepian functions, that can be used for accurate representation and reconstruction of the underlying signal in a given region on the sphere. Using well-optimally concentrated Slepian functions, which have varying energy concentration within a region on the sphere, we propose a transform, referred to as the spatial-Slepian transform (SST), which is similar in formulation to the scale-discretized wavelet transform [30] but uses bandlimited and spatially well-optimally concentrated Slepian functions instead of wavelet functions. Unlike the scale-discretized wavelet transform, spatial-Slepian transform probes local content of the signal (which is a direct consequence of the use of well-optimally concentrated Slepian functions) and results in spatial-Slepian coefficients, which constitute a novel joint spatial-Slepian domain representation of signals on the sphere. The number of spatial-Slepian coefficients is determined by the fractional area of the region chosen to solve the Slepian spatial-spectral concentration problem. In this context, we summarize the main contributions of our work below:

- We use bandlimited and spatially well-optimally concentrated Slepian functions to formulate the spatial-Slepian transform as the inner product between the signal and the rotated Slepian functions in Section III, where we also present the inverse transform to recover the signal from its spatial-Slepian coefficients. Furthermore, we present an algorithm for fast computation of SST by using the framework developed in [37].
- We numerically validate the inverse spatial-Slepian transform using different realizations of a random test signal at various bandlimits in Section IV, and perform computational complexity analysis of the fast algorithm for computing SST. We also quantify the spatial variance of spatial-Slepian coefficients and conduct differ-

A. Aslam and Z. Khalid are with the Department of Electrical Engineering, Syed Babar Ali School of Science and Engineering, Lahore University of Management Sciences, Lahore, Pakistan. A. Aslam is supported by Syed Babar Ali Research Awards.

E-mail: adeem.aslam@lums.edu.pk, zubair.khalid@lums.edu.pk

This article has been accepted for publication in a future issue of this journal, but has not been fully edited. Content may change prior to final publication. Citation information: DOI 10.1109/TSP.2021.3093260, IEEE Transactions on Signal Processing

ent experiments to show that spatial-Slepian coefficients have better spatial localization compared to the scale-discretized wavelet coefficients. Moreover, we present analytical expressions for the spatial-Slepian coefficients computed using zonal Slepian functions for the axisymmetric north polar cap region and present an illustration on a bandlimited Earth topography map.
- In Section V, we present an application of the proposed SST by developing a framework for the detection of hidden localized variations in the signal. We compare the results obtained from the proposed transform with those obtained from the scale-discretized wavelet transform and show that spatial-Slepian transform provides a much better estimate of the underlying region of hidden localized variations on the sphere.

Before formulating the spatial-Slepian transform, we review the necessary mathematical background for signal analysis on the sphere and briefly discuss the Slepian spatial-spectral concentration problem in the next section.

II. Mathematical Background

A. Signals on the 2-Sphere

We consider complex-valued and square-integrable functions on the surface of the 2-sphere (or sphere for short) that is defined as $\mathbb{S}^2 \triangleq \{\hat{\boldsymbol{x}} \in \mathbb{R}^3 \colon |\hat{\boldsymbol{x}}| = 1\}$, where $|\cdot|$ denotes the Euclidean norm, $\hat{\boldsymbol{x}} \equiv \hat{\boldsymbol{x}}(\theta, \phi) \triangleq (\sin\theta\,\cos\phi, \sin\theta\,\sin\phi, \cos\theta)^{\mathrm{T}}$ is a unit vector in $\mathbb{R}^3$, which is parameterized by colatitude $\theta \in [0, \pi]$, measured from positive z-axis, and longitude $\phi \in [0, 2\pi)$, measured from positive x-axis in the $x - y$ plane, and $(\cdot)^{\mathrm{T}}$ denotes the vector transpose. We denote such functions by $f(\hat{\boldsymbol{x}}) \equiv f(\theta, \phi)$ and define the inner product between any two functions $f(\hat{\boldsymbol{x}}), h(\hat{\boldsymbol{x}})$ as [38]

$$\langle f, h\rangle_{\mathbb{S}^2} \triangleq \int_{\mathbb{S}^2} f(\hat{\boldsymbol{x}})\overline{h(\hat{\boldsymbol{x}})}\, ds(\hat{\boldsymbol{x}}), \qquad \int_{\mathbb{S}^2} = \int_{\theta=0}^{\pi}\int_{\phi=0}^{2\pi}, \tag{1}$$

where $\overline{(\cdot)}$ denotes complex conjugate and $ds(\hat{\boldsymbol{x}}) = \sin\theta\, d\theta\, d\phi$ is the differential area element on the sphere. Equipped with the inner product in (1), the set of complex-valued and square-integrable functions on the sphere forms a Hilbert space, denoted by $L^2(\mathbb{S}^2)$. Norm of the function $f(\hat{\boldsymbol{x}})$ is induced by the inner product as $\|f\|_{\mathbb{S}^2} \triangleq \langle f, f\rangle_{\mathbb{S}^2}^{1/2}$ and its energy is given by $\|f\|_{\mathbb{S}^2}^2$. Functions with finite energy are referred to as signals on the sphere. For a given spatial region $R \subset \mathbb{S}^2$, we also define

$$\langle f, h\rangle_R = \int_R f(\hat{\boldsymbol{x}})\overline{h(\hat{\boldsymbol{x}})}\, ds(\hat{\boldsymbol{x}}) \tag{2}$$

as the local inner product between $f(\hat{\boldsymbol{x}})$ and $h(\hat{\boldsymbol{x}})$, where $\|f\|_R^2 \triangleq \langle f, f\rangle_R$ quantifies energy of the signal $f(\hat{\boldsymbol{x}})$ in the region R.

The Hilbert space $L^2(\mathbb{S}^2)$ is separable and contains a complete set of orthonormal basis functions called spherical harmonics, which are given by [38]

$$Y_\ell^m(\hat{\boldsymbol{x}}) \equiv Y_\ell^m(\theta, \phi) \triangleq \sqrt{\frac{2\ell+1}{4\pi}\frac{(\ell-m)!}{(\ell+m)!}}\, P_\ell^m(\cos\theta)e^{im\phi}$$

for integer degree $\ell \geq 0$ and integer order $|m| \leq \ell$, where $P_\ell^m(\cos\theta)$ is the associated Legendre polynomial of degree ℓ and order m [38]. As a result, any signal $f \in L^2(\mathbb{S}^2)$ can be expanded as

$$f(\hat{\boldsymbol{x}}) = \sum_{\ell,m}^{\infty}(f)_\ell^m Y_\ell^m(\hat{\boldsymbol{x}}), \qquad \sum_{\ell,m}^{\infty} \equiv \sum_{\ell=0}^{\infty}\sum_{m=-\ell}^{\ell}, \tag{3}$$

where

$$(f)_m^\ell \triangleq \langle f, Y_\ell^m\rangle_{\mathbb{S}^2} = \int_{\mathbb{S}^2} f(\hat{\boldsymbol{x}})\overline{Y_\ell^m(\hat{\boldsymbol{x}})}\, ds(\hat{\boldsymbol{x}}) \tag{4}$$

is the spherical harmonic (or spectral) coefficient of degree ℓ and order m, and forms the spherical harmonic (spectral) domain representation of the signal $f(\hat{\boldsymbol{x}})$. Signal $f \in L^2(\mathbb{S}^2)$ is considered bandlimited to degree L_f if $(f)_\ell^m = 0, \forall\, \ell \geq L_f, |m| \leq \ell$. Set of all such bandlimited signals on the sphere forms an L_f^2-dimensional subspace of $L^2(\mathbb{S}^2)$, denoted by $\mathcal{H}_{L_f}$, and their spectral coefficients can be stored in an $L_f^2 \times 1$ column vector as

$$\mathbf{f} = \Big[(f)_0^0, (f)_1^{-1}, (f)_1^0, (f)_1^1, \ldots, (f)_{L_f-1}^{L_f-1}\Big]^{\mathrm{T}}. \tag{5}$$

B. Signal Rotation on the Sphere

A point on the surface of the sphere can be rotated to any position by sequential application of sub-rotations by angles $\omega \in [0, 2\pi)$ around z-axis, $\vartheta \in [0, \pi]$ around y-axis and $\varphi \in [0, 2\pi)$ around z-axis, following the right-handed convention. The angles ω, ϑ and φ are called Euler angles. Each rotation by an Euler angle is represented by a 3×3 orthogonal rotation matrix and the overall rotation is specified by a matrix $\mathbf{R}$, defined as

$$\mathbf{R} \equiv \mathbf{R}(\varphi, \vartheta, \omega) \triangleq \mathbf{R}_z(\varphi)\mathbf{R}_y(\vartheta)\mathbf{R}_z(\omega), \tag{6}$$

where $\mathbf{R}_y(\vartheta)$ and $\mathbf{R}_z(\omega)$ are the matrices representing rotations by angles ϑ around y-axis and ω around z-axis respectively [38].

Defining ρ as the 3-tuple of Euler angles, i.e., $\rho \triangleq (\varphi, \vartheta, \omega)$, signal rotation on the sphere is specified by a rotation operator $\mathcal{D}_\rho \equiv \mathcal{D}(\varphi, \vartheta, \omega)$, whose action on a signal $f \in L^2(\mathbb{S}^2)$ is defined as the inverse rotation of the spherical coordinate system, i.e.,

$$(\mathcal{D}_\rho f)(\hat{\boldsymbol{x}}) \equiv (\mathcal{D}(\varphi, \vartheta, \omega)f)(\hat{\boldsymbol{x}}) \triangleq f(\mathbf{R}^{-1}\hat{\boldsymbol{x}}), \tag{7}$$

where $\mathbf{R}$ is the rotation matrix in (6). Spectral coefficients of the rotated signal are given by [38]

$$(\mathcal{D}_\rho f)_\ell^m = \sum_{m'=-\ell}^{\ell} D_{m,m'}^\ell(\rho)(f)_\ell^{m'}, \tag{8}$$

where $D_{m,m'}^\ell(\rho)$ is the Wigner-D function, defined as

$$D_{m,m'}^\ell(\rho) \equiv D_{m,m'}^\ell(\varphi, \vartheta, \omega) \triangleq e^{-im\varphi} d_{m,m'}^\ell(\vartheta) e^{-im'\omega} \tag{9}$$

for integer degree ℓ and integer orders $|m|, |m'| \leq \ell$, and $d_{m,m'}^\ell(\vartheta)$ is the Wigner-d function [38]. As a result, the rotated signal is given by the following Fourier expansion

$$(\mathcal{D}_\rho f)(\hat{\boldsymbol{x}}) = \sum_{\ell,m}^{\infty}\sum_{m'=-\ell}^{\ell} D_{m,m'}^\ell(\rho)(f)_\ell^{m'} Y_\ell^m(\hat{\boldsymbol{x}}). \tag{10}$$

This article has been accepted for publication in a future issue of this journal, but has not been fully edited. Content may change prior to final publication. Citation information: DOI 10.1109/TSP.2021.3093260, IEEE Transactions on Signal Processing

C. Signals on the $\mathbb{SO}(3)$ Rotation Group

Group of all proper rotations[1], parameterized by the 3-tuple $\rho = (\varphi, \vartheta, \omega)$, is called the Special Orthogonal group, denoted by $\mathbb{SO}(3)$. Square-integrable and complex-valued functions defined on the $\mathbb{SO}(3)$ rotation group form a Hilbert space $L^2(\mathbb{SO}(3))$ such that the inner product between any two functions $v, w \in L^2(\mathbb{SO}(3))$ is given by

$$\langle v, w\rangle_{\mathbb{SO}(3)} \triangleq \int_{\mathbb{SO}(3)} v(\rho)\overline{w(\rho)}\, d\rho, \qquad \int_{\mathbb{SO}(3)} = \int_{\varphi=0}^{2\pi}\int_{\vartheta=0}^{\pi}\int_{\omega=0}^{2\pi}, \tag{11}$$

where $d\rho = d\varphi \sin\vartheta\, d\vartheta\, d\omega$ is the differential element on the $\mathbb{SO}(3)$ rotation group. Inner product in (11) induces a norm of the function $v \in L^2(\mathbb{SO}(3))$ as $\|v\|_{\mathbb{SO}(3)} \triangleq \langle v, v\rangle_{\mathbb{SO}(3)}^{1/2}$ and its energy is given by $\|v\|_{\mathbb{SO}(3)}^2$. Such finite energy functions are referred to as signals on the $\mathbb{SO}(3)$ rotation group.

The Hilbert space $L^2(\mathbb{SO}(3))$ is separable and has Wigner-D functions as the basis functions, which admit the following orthogonality relation [38]

$$\left\langle D_{m,m'}^{\ell}, D_{q,q'}^{p}\right\rangle_{\mathbb{SO}(3)} = \left(\frac{8\pi^2}{2\ell+1}\right)\delta_{\ell,p}\delta_{m,q}\delta_{m',q'}, \tag{12}$$

where $\delta_{m,n}$ is the Kronecker delta function. Therefore, any signal $v \in L^2(\mathbb{SO}(3))$ can be expanded as

$$v(\rho) = \sum_{\ell,m,m'}^{\infty} (v)_{m,m'}^{\ell}\overline{D_{m,m'}^{\ell}(\rho)}, \quad \sum_{\ell,m,m'}^{\infty} \equiv \sum_{\ell,m}^{\infty}\sum_{m'=-\ell}^{\ell}, \tag{13}$$

where

$$(v)_{m,m'}^{\ell} \triangleq \left(\frac{2\ell+1}{8\pi^2}\right)\left\langle v, \overline{D_{m,m'}^{\ell}}\right\rangle_{\mathbb{SO}(3)} \tag{14}$$

is the $\mathbb{SO}(3)$ spectral coefficient of degree ℓ and orders m, m', which constitutes the spectral domain representation of the signal $v(\rho)$. Signal $v(\rho)$ is called bandlimited to degree L_v if $(v)_{m,m'}^{\ell} = 0, \forall\, \ell \geq L_v, |m|, |m'| \leq \ell$.

D. Spatial-Spectral Concentration on the Sphere

The problem of spatial concentration of bandlimited signals (or equivalently spectral concentration of spatially limited signals) was first investigated by Slepian and his co-authors in their seminal work on time domain signals in 1960s. They optimized a quadratic energy concentration measure to obtain an orthogonal family of strictly bandlimited signals, which were optimally concentrated within a given time interval [39]. This work was later extended to multidimensional Euclidean domain signals [40], [41] and for signals defined on the sphere [31]–[36]. Here, we briefly review the spatial concentration of bandlimited signals on the sphere.

[1]An improper rotation is a reflection or a flip about either some axes or the center of the spherical coordinate system.

To maximize the spatial energy concentration of a bandlimited signal $g \in \mathcal{H}_{L_g}$ in the spatial region $R \subset \mathbb{S}^2$, following measure of the fractional energy is optimized

$$\begin{aligned}\lambda = \frac{\|g\|_R^2}{\|g\|_{\mathbb{S}^2}^2} &= \frac{\displaystyle\int_R \sum_{p,q}^{L_g-1} (g)_p^q Y_p^q(\hat{\boldsymbol{x}}) \overline{\left(\sum_{\ell,m}^{L_g-1} (g)_\ell^m Y_\ell^m(\hat{\boldsymbol{x}})\right)}}{\displaystyle\int_{\mathbb{S}^2} \sum_{p,q}^{L_g-1} (g)_p^q Y_p^q(\hat{\boldsymbol{x}}) \overline{\left(\sum_{\ell,m}^{L_g-1} (g)_\ell^m Y_\ell^m(\hat{\boldsymbol{x}})\right)}} \\ &= \frac{\displaystyle\sum_{\ell,m}^{L_g-1}\sum_{p,q}^{L_g-1} \overline{(g)_\ell^m}(g)_p^q K_{\ell m,pq}}{\displaystyle\sum_{\ell,m}^{L_g-1} |(g)_\ell^m|^2},\end{aligned} \tag{15}$$

where

$$K_{\ell m,pq} \triangleq \int_R \overline{Y_\ell^m(\hat{\boldsymbol{x}})} Y_p^q(\hat{\boldsymbol{x}})\, ds(\hat{\boldsymbol{x}}), \tag{16}$$

and we have used orthonormality of spherical harmonics on the sphere to get the final equality. Adopting the indexing scheme introduced in (5), we define an $L_g^2 \times L_g^2$ matrix $\mathbf{K}$, with elements $K_{\ell m,pq}$ for $0 \leq \ell, p < L_g, |m| \leq \ell, |q| \leq p$, and an $L_g^2 \times 1$ column vector $\mathbf{g}$, with elements $(g)_\ell^m$, to rewrite (15) in matrix form as

$$\lambda = \frac{\mathbf{g}^{\mathrm{H}}\mathbf{K}\mathbf{g}}{\mathbf{g}^{\mathrm{H}}\mathbf{g}}, \tag{17}$$

where $(\cdot)^{\mathrm{H}}$ represents conjugate transpose. Column vectors $\mathbf{g}$, which render λ in (17) stationary, are solution to the following eigenvalue problem

$$\mathbf{K}\mathbf{g} = \lambda\mathbf{g}. \tag{18}$$

From (16), it can be seen that the matrix $\mathbf{K}$ is Hermitian and positive definite, therefore, the eigenvalues λ are real and eigenvectors $\mathbf{g}$ are orthogonal[2]. We index the eigenvalues (and the associated eigenvectors) such that $1 > \lambda_1 \geq \lambda_2 \geq \ldots \geq \lambda_{L_g^2} > 0$. For each spectral domain eigenvector $\mathbf{g}_\alpha$, associated with the eigenvalue λ_α, we obtain a spatial eigenfunction as

$$g_\alpha(\hat{\boldsymbol{x}}) = \sum_{\ell,m}^{L_g-1} (g_\alpha)_\ell^m Y_\ell^m(\hat{\boldsymbol{x}}), \quad 1 \leq \alpha \leq L_g^2. \tag{19}$$

Set of spatial eigenfunctions, $g_\alpha(\hat{\boldsymbol{x}})$, $\alpha = 1, 2, \ldots, L_g^2$, are orthogonal over the spatial region R and orthonormal over the sphere $\mathbb{S}^2$, i.e.,

$$\begin{aligned}\langle g_\alpha, g_\beta\rangle_R &= \mathbf{g}_\alpha^{\mathrm{H}}\mathbf{K}\,\mathbf{g}_\beta = \lambda_\alpha\delta_{\alpha,\beta}, \\ \langle g_\alpha, g_\beta\rangle_{\mathbb{S}^2} &= \mathbf{g}_\alpha^{\mathrm{H}}\,\mathbf{g}_\beta = \delta_{\alpha,\beta}.\end{aligned} \tag{20}$$

These functions serve as an alternate basis for the space of bandlimited signals, i.e, $\mathcal{H}_{L_g}$, and are referred to as Slepian functions. Consequently, any signal $h \in \mathcal{H}_{L_g}$ can be represented as

$$h(\hat{\boldsymbol{x}}) = \sum_{\alpha=1}^{L_g^2} (h)_\alpha g_\alpha(\hat{\boldsymbol{x}}), \quad (h)_\alpha = \langle h, g_\alpha\rangle_{\mathbb{S}^2} = \mathbf{g}_\alpha^{\mathrm{H}}\mathbf{h}, \tag{21}$$

[2]We choose the eigenvectors $\mathbf{g}$ to be orthonormal in this work.

This article has been accepted for publication in a future issue of this journal, but has not been fully edited. Content may change prior to final publication. Citation information: DOI 10.1109/TSP.2021.3093260, IEEE Transactions on Signal Processing

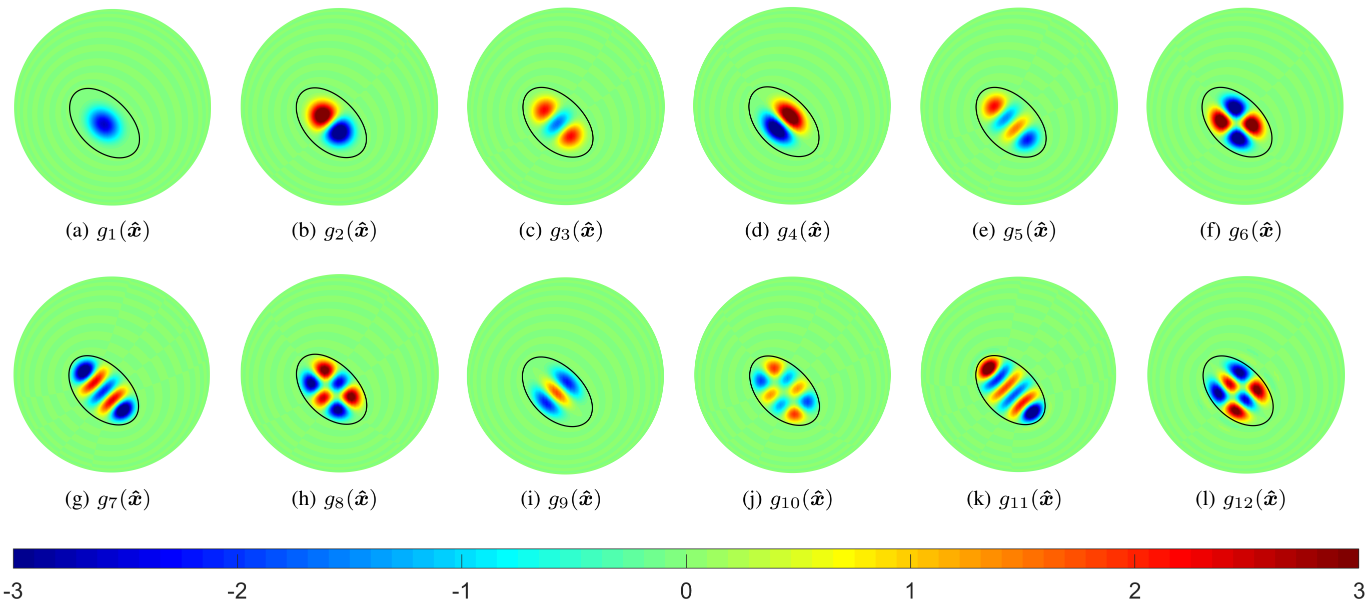

Fig. 1: Real part of Slepian functions computed for a rotated spherical ellipse, which is initially aligned with x-axis, having focus colatitude $\theta_c = 20°$ and semi-major axis $a = 25°$. The rotation angles are $\rho = (60°, 90°, 45°)$ and bandlimit $L_g = 32$.

where $(h)_\alpha$, $\alpha = 1, 2, \ldots, L_g^2$, are called Slepian coefficients, which constitute the Slepian domain representation of the signal $h(\hat{\boldsymbol{x}})$. Fig. 1 shows the real part of the first 12 Slepian functions, bandlimited to degree $L_g = 32$, which are computed for a spherical ellipse[3] that is rotated on the sphere by Euler angles $\rho = (60°, 90°, 45°)$ (the ellipse is initially aligned with x-axis, having focus colatitude $\theta_c = 20°$ and semi-major axis $a = 25°$).

As investigated in detail in [32], if most of the eigenvalues in (18) are either nearly 1 or nearly 0 (suggesting maximal and minimal concentration for the corresponding eigenfunctions in the region R respectively) with a sharp transition, then the sum of eigenvalues, called the spherical Shannon number, is a good measure of the number of well-optimally concentrated Slepian functions within the region R. Denoted by N_R, the spherical Shannon number is given by

$$N_R \triangleq \sum_{\alpha=1}^{L_g^2} \lambda_\alpha = \mathrm{trace}(\mathbf{K}) = \frac{A_R}{4\pi} L_g^2, \tag{22}$$

where $A_R \triangleq \|1\|_R$ is the surface area of the spatial region R. Hence, the first N_R number of well-optimally concentrated Slepian functions in (19) (rounded to the nearest integer) form a (reduced) localized basis set for the accurate reconstruction and representation of bandlimited signals in the spatial region R.

III. Spatial-Slepian Transform (SST)

In this section, we propose the spatial-Slepian transform using well-optimally concentrated Slepian functions. We show that the transform is invertible under some constraints, and present a fast method for the computation of spatial-Slepian coefficients.

A. SST Formulation

The well-optimally concentrated Slepian functions constructed for bandlimit L_g and spatial region R on the sphere, i.e., $g_\alpha(\hat{\boldsymbol{x}}), \alpha = 1, 2, \ldots, N_R$, can be used to obtain a new representation of signals on the sphere through the spatial-Slepian transform[4], which we define as

$$\begin{aligned} F_{g_\alpha}(\rho) &\triangleq \langle f, (\mathcal{D}_\rho g_\alpha)\rangle_{\mathbb{S}^2} \\ &= \int_{\mathbb{S}^2} f(\hat{\boldsymbol{x}}) \overline{(\mathcal{D}_\rho g_\alpha)(\hat{\boldsymbol{x}})}\, ds(\hat{\boldsymbol{x}}) \end{aligned} \tag{23}$$

for a signal $f \in \mathcal{H}_{L_f}$, where $\rho = (\varphi, \vartheta, \omega)$ is the 3-tuple of Euler angles, $\mathcal{D}_\rho \equiv \mathcal{D}(\varphi, \vartheta, \omega)$ is the rotation operator and $F_{g_\alpha} \in L^2(\mathbb{SO}(3))$ is called the α^{th} spatial-Slepian coefficient of the signal $f(\hat{\boldsymbol{x}})$. From its definition, we observe that spatial-Slepian transform probes the signal content by projecting it onto all possible rotated orientations of the well-optimally concentrated Slepian functions on the sphere, essentially spreading the signal in the so called joint spatial-Slepian domain. The extent of the spread of the signal in the joint spatial-Slepian domain, which is quantified by the number of spatial-Slepian coefficients, is specified by the rounded spherical Shannon number, and therefore, depends on the fractional surface area of the region R on the sphere and the bandlimit L_g of the Slepian functions. In this context, we refer to α as the Slepian scale and $F_{g_\alpha}(\rho)$ as the spatial-Slepian coefficient at Slepian scale α.

Using the expansion of signals in (3) and the spectral representation of rotated signals in (8), we can write the

[3] We refer the reader to [42] for the definition of a spherical ellipse.

[4] We use the term spatial-Slepian transform to differentiate it from the Slepian transform, which refers to the inner product between a signal and a Slepian function.

spatial-Slepian coefficient in (23) as

$$F_{g_\alpha}(\rho) = \sum_{\ell,m,m'}^{\min\{L_f-1,L_g-1\}} (f)_\ell^m \overline{(g_\alpha)_\ell^{m'}}\, \overline{D_{m,m'}^\ell(\rho)}, \qquad (24)$$

where we have used orthonormality of spherical harmonics on the sphere to obtain the result.

Remark 1: Spatial-Slepian transform has been formulated using the definition of convolution of signals on the sphere, given in [37]. Such definition of convolution of signals has also been adopted to define the scale-discretized wavelet transform on the sphere [29], [30]. Hence, the spatial-Slepian transform in (23) appears similar in its mathematical formulation to the scale-discretized wavelet transform on the sphere. However, the proposed transform uses Slepian functions, rather than scale-discretized wavelet functions, and results in a joint domain representation which is not only different from the multiscale wavelet representation but is not found in the literature as well, rendering this work a novel research contribution. Since, unlike wavelet functions, Slepian functions are tuned to the underlying local region of interest, the proposed spatial-Slepian transform serves as an invaluable tool for probing the contents of any signal, which is localized within a region on the sphere.

B. Inverse SST

Spectral representation of the spatial-Slepian coefficient $F_{g_\alpha}(\rho)$ is given by

$$(F_{g_\alpha})_{m,m'}^\ell \triangleq \left(\frac{2\ell+1}{8\pi^2}\right)\left\langle F_{g_\alpha}, \overline{D_{m,m'}^\ell}\right\rangle_{\mathbb{SO}(3)} = (f)_\ell^m \overline{(g_\alpha)_\ell^{m'}} \qquad (25)$$

for $0 \le \ell \le \min\{L_f-1, L_g-1\}$, $|m|, |m'| \le \ell$, where we have used (11) and orthogonality of Wigner-D functions on the $\mathbb{SO}(3)$ rotation group to obtain the final result. Hence, we can recover the spectral coefficients of the original signal $f(\hat{\boldsymbol{x}})$ as

$$\begin{aligned}(f)_\ell^m &= \left(\frac{2\ell+1}{8\pi^2}\right)\frac{\left\langle F_{g_\alpha}, \overline{D_{m,m'}^\ell}\right\rangle_{\mathbb{SO}(3)}}{\overline{(g_\alpha)_\ell^{m'}}} \\ &= \left(\frac{2\ell+1}{8\pi^2}\right)\frac{\int_{\mathbb{SO}(3)} F_{g_\alpha}(\rho) D_{m,m'}^\ell(\rho)\, d\rho}{\overline{(g_\alpha)_\ell^{m'}}} \end{aligned}\qquad (26)$$

for $0 \le \ell \le \min\{L_f-1, L_g-1\}$, $|m|, |m'| \le \ell$. From (26), we note that the proposed spatial-Slepian transform is invertible only if the spherical harmonic coefficients of the Slepian function, i.e., $(g_\alpha)_\ell^{m'}$, are non-zero for all degrees $0 \le \ell \le \min\{L_f-1, L_g-1\}$ and at least one order $|m'| \le \ell$.

Remark 2: For the case where $L_f > L_g$, the inverse spatial-Slepian transform cannot recover all of the spectral coefficients of the signal $f(\hat{\boldsymbol{x}})$. On the other hand if $L_f < L_g$, the Slepian functions are under-utilized in obtaining the spatial-Slepian coefficients for the signal $f(\hat{\boldsymbol{x}})$. Therefore, in this work, we assume that $L_f = L_g$, so that not only the Slepian functions are fully utilized, signal $f(\hat{\boldsymbol{x}})$ is also perfectly recovered from its spatial-Slepian coefficients.

C. Fast Computation of Spatial-Slepian Transform

Since the spatial-Slepian transform has been proposed using the definition of convolution of signals on the sphere [37], we adopt the framework for fast computation of convolution of spherical signals, given in [37], to efficiently compute the spatial-Slepian coefficients. This fast algorithm has become a standard tool for efficient computation of transforms which are defined through the inner product between signals on the sphere, such as the directional spatially localized spherical harmonic transform [42] and the scale-discretized wavelet transform on the sphere [43].

From the definition of Wigner-D functions in (9), we note that the spatial-Slepian coefficient in (24) can be written as

$$\begin{aligned} F_{g_\alpha}(\varphi,\vartheta,\omega) &= \sum_{\ell,m,m'}^{L_f-1} (f)_\ell^m\, \overline{(g_\alpha)_\ell^{m'}}\, e^{im\varphi}\, \overline{d_{m,m'}^\ell(\vartheta)}\, e^{im'\omega} \\ &= \sum_{\ell=0}^{L_f-1}\sum_{m=-\ell}^{\ell} (f)_\ell^m e^{im\varphi} \sum_{m'=-\ell}^{\ell} \overline{(g_\alpha)_\ell^{m'}} \times \\ &\qquad i^{m'-m} e^{im'\omega} \sum_{m''=-\ell}^{\ell} \Delta_{m'',m}^\ell\, \Delta_{m'',m'}^\ell e^{im''\vartheta}, \end{aligned} \qquad (27)$$

where $\Delta_{m,m'}^\ell \triangleq d_{m,m'}^\ell(\pi/2)$ and we have used the following expansion for Wigner-d functions [38],

$$d_{m,m'}^\ell(\vartheta) = i^{m-m'} \sum_{m''=-\ell}^{\ell} \Delta_{m'',m}^\ell \Delta_{m'',m'}^\ell e^{-im''\vartheta}. \qquad (28)$$

Rearranging the summations in (27), we can rewrite the spatial-Slepian coefficient as

$$F_{g_\alpha}(\rho) = \sum_{m,m',m''=-(L_f-1)}^{L_f-1} C_{m,m',m''}^\alpha e^{i(m\varphi+m''\vartheta+m'\omega)}, \qquad (29)$$

where

$$C_{m,m',m''}^\alpha = i^{m'-m} \sum_{\ell=\max\{|m|,|m'|,|m''|\}}^{L_f-1} (f)_\ell^m\, \overline{(g_\alpha)_\ell^{m'}}\, \Delta_{m'',m}^\ell \Delta_{m'',m'}^\ell. \qquad (30)$$

The expression in (29) is a simple rearrangement of the initial expression in (24) and hence, is not more efficient. However, the presence of complex exponential functions in (29) facilitates the use of the fast Fourier transform (FFT) algorithm to compute the spatial-Slepian coefficient efficiently. Wigner-d functions $\Delta_{m,m'}^\ell$ can be computed using either the recursive relations given in [44] or the recursion proposed in [45], both of which are stable up to very large degrees.

IV. Analysis

In this section, we validate the inverse spatial-Slepian transform in (26), using different realizations of a random test signal at various bandlimits, and perform computational complexity analysis of the fast algorithm presented in Section III-C. Moreover, we quantify the spatial variance of spatial-Slepian coefficients and conduct different experiments

This article has been accepted for publication in a future issue of this journal, but has not been fully edited. Content may change prior to final publication. Citation information: DOI 10.1109/TSP.2021.3093260, IEEE Transactions on Signal Processing

to show that spatial-Slepian coefficients have better spatial localization than scale-discretized wavelet coefficients. We also present illustrations of the spatial-Slepian coefficients of a bandlimited Earth topography map using the specialized case of zonal Slepian functions, which are computed for the axisymmetric north polar cap region on the sphere.

A. Inverse SST Validation

We analyze the accuracy of the inverse SST using different realizations of a random, complex-valued test signal $f^T(\hat{\boldsymbol{x}})$, whose spectral coefficients are uniformly distributed in the interval $(-1,1)$ in both real and imaginary parts. We compute the spectral components of the spatial-Slepian coefficients of the test signal, i.e., $\left(F^T_{g_\alpha}\right)^\ell_{m,m'}$, from (25) using Slepian functions that are well-optimally concentrated in an axisymmetric north polar cap region, defined as $\{\hat{\boldsymbol{x}}(\theta,\phi) \in \mathbb{R}^3 : |\hat{\boldsymbol{x}}| = 1, 0 \le \theta \le \Theta_c, 0 \le \phi < 2\pi\}$, where $\Theta_c \in [0,\pi/2]$ is the polar cap angle which is set to $15°$ in this experiment. Spectral coefficients of the reconstructed signal, denoted by $(f^R)^m_\ell$, are computed from the inverse SST in (26) using the Slepian function at Slepian scale $\alpha = 1$, i.e.,

$$(f^R)^m_\ell = \frac{\left(F^T_{g_1}\right)^\ell_{m,m'}}{\overline{(g_1)^{m'}_\ell}}, \quad |m| \le \ell, 0 \le \ell < L_f, \tag{31}$$

where L_f is the bandlimit of the test signal. Numerical accuracy of the inverse SST is evaluated by defining the absolute mean error as follows

$$\mathbf{E}_{\text{mean}} = \frac{1}{L_f^2} \sum_{\ell,m}^{L_f-1} \left|(f^T)^m_\ell - (f^R)^m_\ell\right|, \tag{32}$$

which is averaged over 100 different realizations of the test signal. The results of this experiment are shown in Fig. 2 at different values of the bandlimit L_f. As expected, average absolute mean error is on the order of numerical precision, which in turn establishes the numerical stability of the proposed inverse SST.

B. Computational Complexity Analysis

We observe that spatial-Slepian transform in (29) requires the computation of coefficients $C^\alpha_{m,m',m''}$ over the three dimensional space of orders m, m' and m''. Coefficients $C^\alpha_{m,m',m''}$ in turn require a single summation over the degree ℓ for each m, m', m''. As a result, the complexity of computing $C^\alpha_{m,m',m''}$ scales as $O(L_f^4)$ with bandlimit L_f. We further note that Wigner-d functions $\Delta^\ell_{m,m'}$ do not depend on either the signal or Slepian functions and hence, can be independently computed in time which scales as $O(L_f^3)$, using the recursion in [44]. However, we compute $\Delta^\ell_{m,m'}$ on-the-fly to minimize storage requirements and note that this does not change the computational complexity of $O(L_f^4)$ for the coefficients $C^\alpha_{m,m',m''}$. Computational complexity of the three dimensional fast Fourier transform scales as $O(L_f^3 \log_2 L_f)$ with bandlimit L_f. Hence, the overall complexity for computing the spatial-Slepian coefficient in (29) is governed by the coefficients $C^\alpha_{m,m',m''}$, and is given by $O(L_f^4)$ for a fixed Slepian scale α, and $O(N_R L_f^4)$ for all Slepian scales, i.e., $\alpha = 1, 2, \ldots, N_R$.

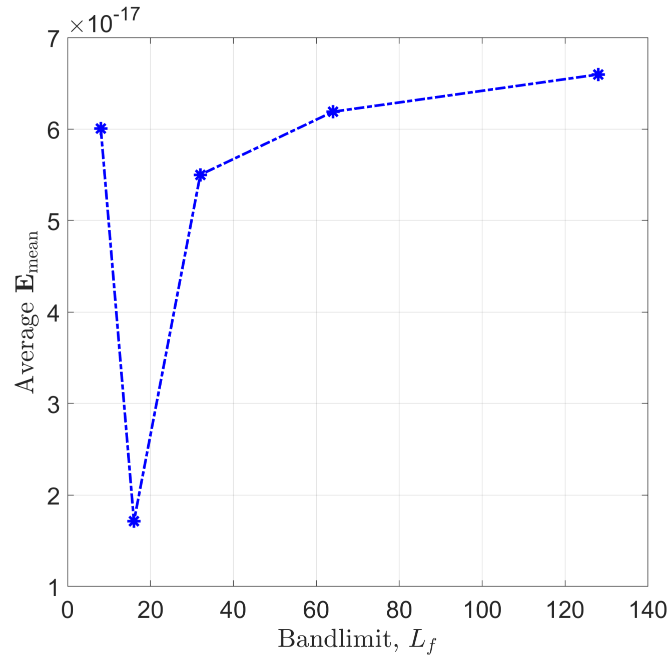

Fig. 2: Absolute mean error $\mathbf{E}_{\text{mean}}$, computed between the spectral coefficients of a random, complex-valued test signal $f^T(\hat{\boldsymbol{x}})$ and the reconstructed signal $f^R(\hat{\boldsymbol{x}})$, is averaged over 100 different realizations of the test signal and plotted against the signal bandlimit $8 \le L_f \le 128$. Figure shows that the error is on the order of numerical precision, which in turn verifies the numerical stability of the proposed inverse SST.

We validate the computational complexity of the spatial-Slepian transform using one of the Slepian functions (at Slepian scale $\alpha = 1$), computed for a spherical ellipse which is aligned with x-axis, having focus colatitude $\theta_c = 15°$ and semi-major axis $a = 20°$. Spatial-Slepian transform is computed for a test signal, which is generated in the spectral domain in such a way the spectral coefficients are complex, with real and imaginary parts uniformly distributed in the interval $(0,1)$. The experiment is performed in MATLAB, running on a 2.2 GHz Intel Core i7 processor with 16 GB RAM, for 10 different realizations of the test signal. We record the mean time (averaged over 10 realizations) at different values of the bandlimit L_f and plot it in Fig. 3, where we have also shown the theoretical bound which scales as $O(L_f^4)$. As expected, the results in Fig. 3 corroborate the theoretically established bound on the computational complexity of the spatial-Slepian transform.

C. Variance of the Spatial-Slepian Coefficients

We adopt the formulation of spatial variance presented in [46] to quantify the localization of spatial-Slepian coefficients on the $\mathbb{SO}(3)$ rotation group as

$$\text{var}_{F_{g_\alpha}(\rho)} = \mu_{|F_{g_\alpha}(\rho)|^2} - \left|\mu_{F_{g_\alpha}(\rho)}\right|^2, \tag{33}$$

This article has been accepted for publication in a future issue of this journal, but has not been fully edited. Content may change prior to final publication. Citation information: DOI 10.1109/TSP.2021.3093260, IEEE Transactions on Signal Processing

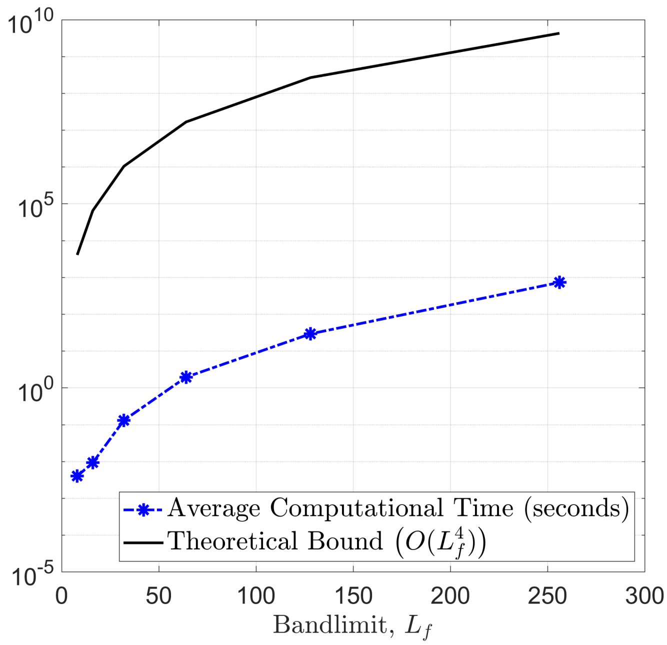

Fig. 3: Computational complexity analysis of the spatial-Slepian transform for a test signal using Slepian function at Slepian scale $\alpha = 1$, computed for a spherical ellipse which is aligned with x-axis, having focus colatitude $\theta_c = 15°$ and semi-major axis $a = 20°$. Computational time (shown in blue), which is averaged over 10 different realizations of the test signal, is in agreement with the theoretical bound of $O(L_f^4)$ (shown in black).

where $\mu_{f(\rho)}$ is the spatial mean of a function $f \in L^2(\mathbb{SO}(3))$ and is defined as

$$\mu_{f(\rho)} \triangleq \frac{1}{8\pi^2} \int_{\mathbb{SO}(3)} f(\rho) d\rho. \tag{34}$$

Using the expression for Wigner-D functions in (9) and the following relation between Wigner-d functions and Legendre polynomials [38]

$$d^{\ell}_{m,0}(\vartheta) = \sqrt{\frac{(\ell - m)!}{(\ell + m)!}} P_\ell(\cos\vartheta), \tag{35}$$

we obtain the mean of the spatial-Slepian coefficients over the $\mathbb{SO}(3)$ rotation group as

$$\begin{aligned}
\mu_{F_{g_\alpha}(\rho)} &= \sum_{\ell,m,m'}^{L_f-1} (f)^m_\ell \overline{(g_\alpha)^{m'}_\ell} \mu_{\overline{D^\ell_{m,m'}(\rho)}} \\
&= \sum_{\ell,m,m'}^{L_f-1} (f)^m_\ell (g_\alpha)^{m'}_\ell \frac{1}{8\pi^2} \int_{\mathbb{SO}(3)} \overline{D^\ell_{m,m'}(\rho)} d\rho \\
&= \sum_{\ell,m,m'}^{L_f-1} (f)^m_\ell \overline{(g_\alpha)^{m'}_\ell} \frac{1}{2} \delta_{m,0}\delta_{m',0} \int_{\cos\vartheta=-1}^{1} P_\ell(\cos\vartheta) d(\cos\vartheta) \\
&= \sum_{\ell,m,m'}^{L_f-1} (f)^m_\ell \overline{(g_\alpha)^{m'}_\ell} \delta_{m,0}\, \delta_{m',0}\, \delta_{\ell,0} = (f)^0_0 \overline{(g_\alpha)^0_0}.
\end{aligned} \tag{36}$$

Hence, spatial variance of the spatial-Slepian coefficient at Slepian scale α becomes

$$\begin{aligned}
\mathrm{var}_{F_{g_\alpha}(\rho)} &= \mu_{|F_{g_\alpha}(\rho)|^2} - \left|(f)^0_0\right|^2 \left|(g_\alpha)^0_0\right|^2 \\
&= \sum_{\ell,m,m'}^{L_f-1} (f)^m_\ell \overline{(g_\alpha)^{m'}_\ell} \sum_{p,q,q'}^{L_f} \overline{(f)^q_p} (g_\alpha)^{q'}_p \times \\
&\qquad \mu_{\overline{D^\ell_{m,m'}(\rho)} D^p_{q,q'}(\rho)} - \left|(f)^0_0\right|^2 \left|(g_\alpha)^0_0\right|^2 \\
&= \sum_{\ell,m,m'}^{L_f-1} \left(\frac{1}{2\ell+1}\right) |(f)^m_\ell|^2 \left|(g_\alpha)^{m'}_\ell\right|^2 - \left|(f)^0_0\right|^2 \left|(g_\alpha)^0_0\right|^2,
\end{aligned} \tag{37}$$

where we have used orthogonality of Wigner-D functions on $\mathbb{SO}(3)$ rotation group to obtain the final result. As is evident from the expression in (37), variance of the spatial-Slepian coefficient depends on the signal under consideration in addition to the Slepian function.

We compute the spatial variance of the spatial-Slepian coefficients for the Earth topography map[5], bandlimited to degree $L_f = 64$, using the Slepian functions which are well-optimally concentrated in the axisymmetric north polar cap region R. For comparison, we also evaluate the spatial variance of scale-discretized wavelet coefficients of the bandlimited Earth topography map, which is given by [46]

$$\mathrm{var}_{w_f^{\Psi^{(s)}}(\rho)} = \sum_{\ell,m,m'}^{L_f-1} \left(\frac{1}{2\ell+1}\right) |(f)^m_\ell|^2 \left|\left(\Psi^{(s)}\right)^{m'}_\ell\right|^2, \tag{38}$$

where $\Psi^{(s)} \in L^2(\mathbb{S}^2)$ is the wavelet function at wavelet scale s, having azimuthal bandlimit L_ϕ[6], $w_f^{\Psi^{(s)}}(\rho)$ is the corresponding scale-discretized wavelet coefficient, given by [30]

$$w_f^{\Psi^{(s)}}(\rho) = \left\langle f, \left(\mathcal{D}_\rho \Psi^{(s)}\right)\right\rangle_{\mathbb{S}^2} = \int_{\mathbb{S}^2} f(\hat{\boldsymbol{x}}) \overline{\left(\mathcal{D}_\rho \Psi^{(s)}(\hat{\boldsymbol{x}})\right)} ds(\hat{\boldsymbol{x}}), \tag{39}$$

and we have used the fact that $\left(\Psi^{(s)}\right)^0_0 = 0$. The minimum wavelet scale is chosen to be 0 and the maximum wavelet scale depends on the bandlimit as [30]

$$s_{\max} = \lceil \log_\gamma(L_f) \rceil, \tag{40}$$

where γ is the harmonic space dilation parameter of the scale-discretized wavelet functions. We relate the polar cap angle of the north polar cap region R to the dilation parameter γ in such a way that the number of wavelet scales equals the number of Slepian scales, i.e.,

$$N_R = \frac{2\pi(1-\cos\Theta_c)}{4\pi} L_f^2 = s_{\max} + 1 = \lceil \log_\gamma(L_f) \rceil + 1. \tag{41}$$

We set $\gamma = 2$ which results in the maximum wavelet scale $s_{\max} = 6$, $N_R = 7$ and the polar cap angle $\Theta_c = 4.7°$. Spatial variance of spatial-Slepian coefficients and scale-discretized wavelet coefficients, for the bandlimited Earth topography

[5]http://geoweb.princeton.edu/people/simons/software.html

[6]The azimuthal bandlimit L_ϕ is set to 5 for this experiment. For a detailed treatment of scale-discretized wavelet transform on the sphere, we refer the reader to [30].

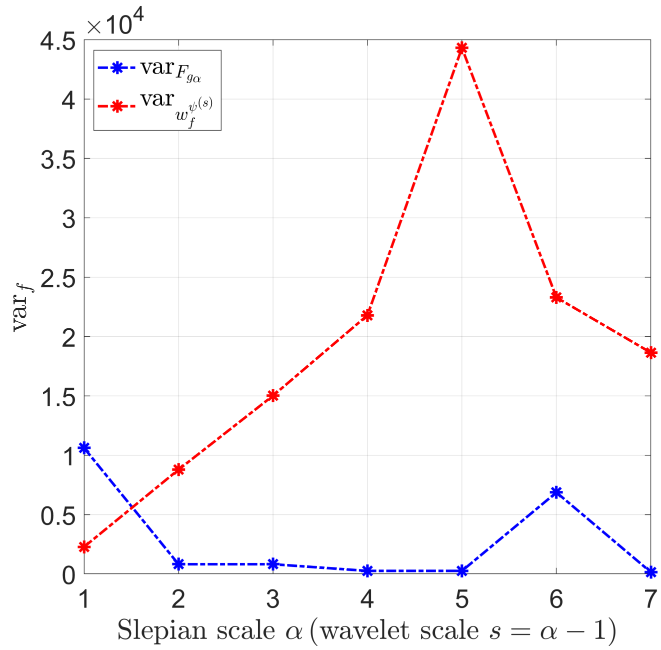

Fig. 4: Spatial variance of spatial-Slepian and scale-discretized wavelet coefficients, evaluated for the Earth topography map bandlimited to degree $L_f = 64$. Spatial-Slepian coefficients can be seen to be better localized than scale-discretized wavelet coefficients at most of the scales.

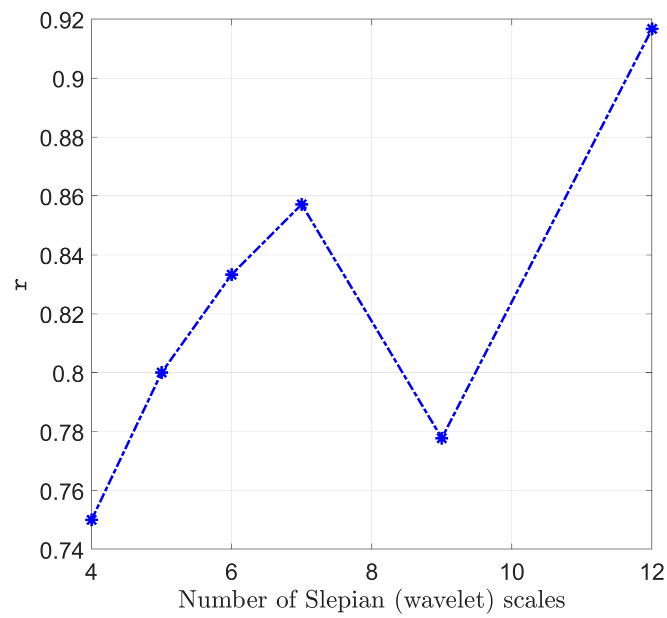

Fig. 5: Fractional ratio $\mathtt{r}$, for the Earth topography map bandlimited to degree $L_f = 64$, is plotted against different number of Slepian (wavelet) scales, which are obtained by varying the polar cap angle Θ_c and the dilation parameter γ in such a way that the number of Slepian scales equals the number of wavelet scales. The curve shows that more number of spatial-Slepian coefficients have smaller spatial variance (and hence, better spatial localization) than the scale-discretized wavelet coefficients.

map, is computed at each Slepian and wavelet scale and plotted in Fig. 4. Spatial variance of the spatial-Slepian coefficients can be seen to be smaller than that of the scale-discretized wavelet coefficients at most of the scales, which is evidence of better spatial localization of the spatial-Slepian coefficients compared to the scale-discretized wavelet coefficients.

We vary the dilation parameter of the wavelet functions while keeping the bandlimit the same, i.e., $L_f = 64$, to obtain different number of wavelet scales for the scale-discretized wavelet transform of the Earth topography map. We also compute spatial-Slepian coefficients of the Earth topography map using the well-optimally concentrated Slepian functions for the north polar cap region with varying polar cap angles in such a way that the number of Slepian scales equals the number of wavelet scales, according to (41). The fractional ratio of the number of spatial-Slepian coefficients (at each polar cap angle Θ_c) having smaller spatial variance than the scale-discretized wavelet coefficients (at each dilation parameter γ) is quantified as

$$\mathtt{r}(\Theta_c) \triangleq \frac{\#\left\{\mathrm{var}_{F_{g_\alpha}(\rho)} \leq \mathrm{var}_{w_f^{\Psi(s)}(\rho)}\right\}}{N_R}, \quad N_R \equiv N_R(\Theta_c), \tag{42}$$

where $\#\{\cdot\}$ computes the number of elements satisfying the logical condition within the braces and N_R is the number of Slepian scales (which is equal to the number of wavelet scales). For dilation parameter $\gamma = 1.5, 1.8, 2, 2.5, 3, 4$, we obtain the polar cap angles, using (41), as $\Theta_c = 6.2°, 5.4°, 4.7°, 4.4°, 4°, 3.6°$, such that the number of corresponding Slepian (or wavelet) scales are $12, 9, 7, 6, 5, 4$. The resulting fractional ratio $\mathtt{r}$ is plotted against the number of Slepian (wavelet) scales in Fig. 5, which shows that more number of spatial-Slepian coefficients have smaller spatial variance than the scale-discretized wavelet coefficients.

D. SST using Zonal Slepian Functions for Axisymmetric North Polar Cap Region

Slepian spatial-spectral concentration problem for polar cap regions has been investigated and analytically solved in [32]. In particular, we use the order $m = 0$ Slepian functions, which are axisymmetric, i.e., $g_\alpha(\theta, \phi) = g_\alpha(\theta)$, and are called zonal Slepian functions, to compute the spatial-Slepian transform. Spherical Shannon number for zonal Slepian functions is denoted by $N_{\Theta_c,0}$ and is given by [12]

$$N_{\Theta_c,0} = L_f \frac{\Theta_c}{\pi}. \tag{43}$$

Using the following spectral representation for zonal Slepian functions [38]

$$(g_\alpha)_\ell^m = (g_\alpha)_\ell^0 \delta_{m,0}, \tag{44}$$

we can write the rotated Slepian function $(\mathcal{D}_\rho g_\alpha)(\hat{\boldsymbol{x}})$ in (23) as

$$(\mathcal{D}_\rho g_\alpha)(\hat{\boldsymbol{x}}) = \sum_{\ell,m}^{L_f-1} \sqrt{\frac{4\pi}{2\ell+1}}\, \overline{Y_\ell^m(\vartheta,\varphi)}(g_\alpha)_\ell^0 Y_\ell^m(\hat{\boldsymbol{x}}), \tag{45}$$

This article has been accepted for publication in a future issue of this journal, but has not been fully edited. Content may change prior to final publication. Citation information: DOI 10.1109/TSP.2021.3093260, IEEE Transactions on Signal Processing

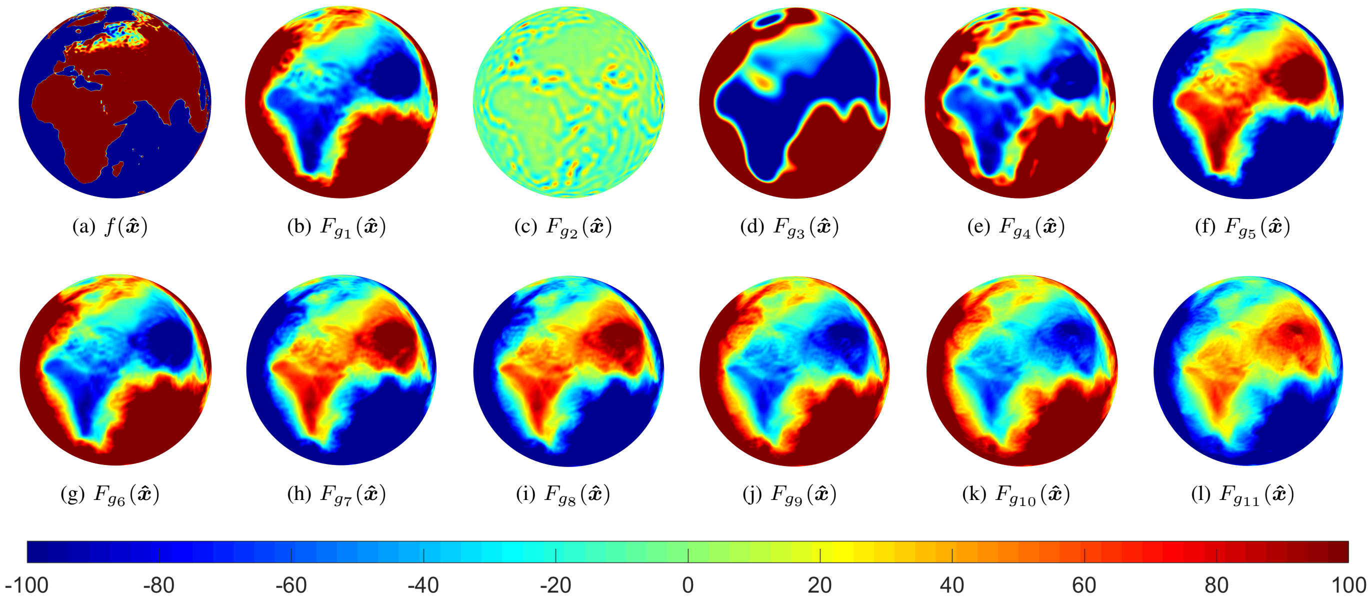

(a) $f(\hat{\boldsymbol{x}})$ (b) $F_{g_1}(\hat{\boldsymbol{x}})$ (c) $F_{g_2}(\hat{\boldsymbol{x}})$ (d) $F_{g_3}(\hat{\boldsymbol{x}})$ (e) $F_{g_4}(\hat{\boldsymbol{x}})$ (f) $F_{g_5}(\hat{\boldsymbol{x}})$

(g) $F_{g_6}(\hat{\boldsymbol{x}})$ (h) $F_{g_7}(\hat{\boldsymbol{x}})$ (i) $F_{g_8}(\hat{\boldsymbol{x}})$ (j) $F_{g_9}(\hat{\boldsymbol{x}})$ (k) $F_{g_{10}}(\hat{\boldsymbol{x}})$ (l) $F_{g_{11}}(\hat{\boldsymbol{x}})$

Fig. 6: Earth topography map and $N_{\Theta_c,0} \approx 11$ spatial-Slepian coefficients for the Earth topography map at bandlimit $L_f = 128$ using zonal Slepian functions, which are computed for an axisymmetric north polar cap region of polar cap angle $\Theta_c = 15°$.

where we have used the fact that for $m' = 0$ the first rotation by ω around z-axis has no effect and can be taken to be 0, along with the following relation [38], to obtain the final result

$$D^{\ell}_{m,0}(\varphi,\vartheta,0) = \sqrt{\frac{4\pi}{2\ell+1}}\,\overline{Y^m_\ell(\vartheta,\varphi)}. \tag{46}$$

Therefore, employing orthonormality of spherical harmonics on the sphere, SST in (23), using zonal Slepian functions computed for an axisymmetric polar cap region, can be rewritten as

$$\begin{aligned} F_{g_\alpha}(\rho) &= \langle f, (\mathcal{D}_\rho g_\alpha)\rangle_{\mathbb{S}^2} \\ &= \sum_{\ell,m}^{L_f-1} \sqrt{\frac{4\pi}{2\ell+1}}(f)^m_\ell \overline{(g_\alpha)^0_\ell}\, Y^m_\ell(\vartheta,\varphi) = F_{g_\alpha}(\vartheta,\varphi). \end{aligned} \tag{47}$$

Note that the spatial-Slepian coefficient, in this case, is a signal on the sphere $\mathbb{S}^2$, with spherical harmonic coefficients given by

$$(F_{g_\alpha})^m_\ell = \langle F_{g_\alpha}, Y^m_\ell\rangle_{\mathbb{S}^2} = \sqrt{\frac{4\pi}{2\ell+1}}(f)^m_\ell \overline{(g_\alpha)^0_\ell}. \tag{48}$$

As a result, signal $f(\hat{\boldsymbol{x}})$ can be reconstructed perfectly from the spatial-Slepian coefficients as

$$f(\theta,\phi) = \sum_{\ell,m}^{L_f-1}\left[\sqrt{\frac{2\ell+1}{4\pi}}\frac{\langle F_{g_\alpha}, Y^m_\ell\rangle_{\mathbb{S}^2}}{\overline{(g_\alpha)^0_\ell}}\right] Y^m_\ell(\theta,\phi), \tag{49}$$

for $\overline{(g_\alpha)^0_\ell} \neq 0, \forall\, \ell < L_f$. We use the Earth topography map, bandlimited to degree $L_f = 128$, for the computation of spatial-Slepian transform using the zonal Slepian functions, which are computed for an axisymmetric north polar cap region of polar cap angle $\Theta_c = 15°$. Fig. 6 shows the spatial-Slepian coefficients for the first $N_{\Theta_c,0} \approx 11$ Slepian scales, along with the Earth topography map.

V. Localized Variation Analysis

As discussed in Section II-D, bandlimited Slepian functions form an alternative basis set for the representation of bandlimited signals on the sphere, and well-optimally concentrated bandlimited Slepian basis functions form a (reduced) localized basis set for accurate representation and reconstruction of bandlimited signals over a region on the sphere. Hence, this reduced basis can prove to be an invaluable tool for probing the contents of any signal, which is localized within a region on the sphere. In this context, we present an application of the spatial-Slepian transform, by utilizing it for detecting hidden variations in a signal, which are localized within an unknown region on the sphere. The objective is to detect the presence of these variations along with an estimate of the underlying region that these variations are localized within. In the remainder of this section, we elaborate on the problem of localized variation analysis and show that it is motivated by an application in the field of medical imaging. We then formulate a mathematical framework for localized variation analysis using spatial-Slepian transform, and use a toy example for illustration. We compare the results obtained from the spatial-Slepian transform with those obtained from the scale-discretized wavelet transform, and show that spatial-Slepian transform performs better by achieving a better estimate of the underlying region of localized variations.

A. Motivation

The problem of localized variation analysis is motivated by an application in the field of medical imaging, in which images of a human organ, e.g., the brain, are analyzed across different patients to diagnose the growth of a hidden anomaly, i.e., a tumor, which is not readily apparent in the images. The tumor can be effectively modeled as a variation that is

This article has been accepted for publication in a future issue of this journal, but has not been fully edited. Content may change prior to final publication. Citation information: DOI 10.1109/TSP.2021.3093260, IEEE Transactions on Signal Processing

hidden in the spherical image of the brain. We refer to the scan of the healthy brain, i.e., without the anomaly, as the source signal $b(\hat{\boldsymbol{x}})$, which is unknown. The anomaly is modeled as an extremely weak localized variation $v(\hat{\boldsymbol{x}})$, which is hidden in the source signal $b(\hat{\boldsymbol{x}})$ to give the scan of the brain as the spherical observation $f(\hat{\boldsymbol{x}}) = b(\hat{\boldsymbol{x}}) + v(\hat{\boldsymbol{x}})$, $\|v\|_{\mathbb{S}^2} \ll \|b\|_{\mathbb{S}^2}$. We assume that N different patients take part in this medical study, resulting in N different instances (realizations) of such a localized variation, which gives us an ensemble of observations as

$$f^j(\hat{\boldsymbol{x}}) = b(\hat{\boldsymbol{x}}) + v^j(\hat{\boldsymbol{x}}), \qquad j = 1, 2, \ldots, N. \tag{50}$$

The objective is to statistically identify the portion of the brain which has been affected by the tumor.

B. Mathematical Framework

We compute spatial-Slepian coefficients of the observations using the well-optimally concentrated Slepian functions in a region R on the sphere. From linearity of the spatial-Slepian transform, we can write the spatial-Slepian coefficient of j^{th} observation as

$$F^j_{g_\alpha}(\rho) = B_{g_\alpha}(\rho) + V^j_{g_\alpha}(\rho), \qquad \alpha = 1, 2, \ldots, N_R, \tag{51}$$

with statistical mean and variance given by

$$\mathbb{E}\left\{F_{g_\alpha}(\rho)\right\} = B_{g_\alpha}(\rho) + \mathbb{E}\left\{V_{g_\alpha}(\rho)\right\} \tag{52}$$

and

$$\begin{aligned}\sigma^2_{F_{g_\alpha}}(\rho) &= \mathbb{E}\left\{\left|F_{g_\alpha}(\rho) - \mathbb{E}\left\{F_{g_\alpha}(\rho)\right\}\right|^2\right\} \\ &= \mathbb{E}\left\{\left|V_{g_\alpha}(\rho)\right|^2\right\} - \left|\mathbb{E}\left\{V_{g_\alpha}(\rho)\right\}\right|^2 = \sigma^2_{V_{g_\alpha}}(\rho)\end{aligned} \tag{53}$$

respectively, where $\mathbb{E}\{\cdot\}$ denotes the expectation operator. We observe that spatial-Slepian coefficients of the observation have same variance as the spatial-Slepian coefficients of the localized variations, which enables us to use the sample variance across different instances, denoted by $\Sigma^2_{F_{g_\alpha}}$ and given by

$$\Sigma^2_{F_{g_\alpha}}(\rho) = \frac{1}{N}\sum_{j=1}^{N}\left|F^j_{g_\alpha}(\rho) - \frac{1}{N}\sum_{j=1}^{N}F^j_{g_\alpha}(\rho)\right|^2, \tag{54}$$

as a statistical measure for detecting the presence of hidden localized variations in the signal at different Slepian scales α.

C. Illustration

As an illustration, we consider a realization of a zero-mean and anisotropic Gaussian process as the background source signal $b(\hat{\boldsymbol{x}})$, with bandlimit $L_b = 32$. We generate localized variations within the region $\tilde{R}$, which is taken to be a spherical ellipse, initially aligned with x-axis having focus colatitude $\theta_c = 20°$ and semi-major axis $a = 25°$, that is rotated by the Euler angles $\rho = (60°, 90°, 45°)$. The localized variations are given by

$$v^j(\hat{\boldsymbol{x}}) = \sum_{\beta=1}^{N_{\tilde{R}}\approx 30} a^j_\beta \tilde{g}_\beta(\hat{\boldsymbol{x}}), \tag{55}$$

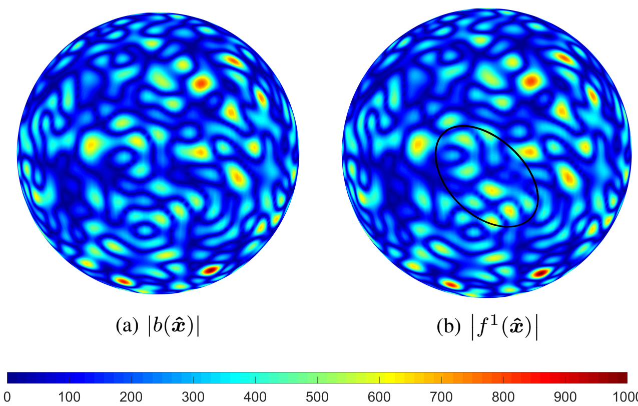

(a) $|b(\hat{\boldsymbol{x}})|$ (b) $|f^1(\hat{\boldsymbol{x}})|$

Fig. 7: Magnitude of (a) the source signal, which is a realization of a zero-mean and anisotropic Gaussian process, and (b) the first observation that contains localized variation hidden in the source signal within the elliptical region. Both signals are bandlimited to degree 32.

where $\tilde{g}_\beta(\hat{\boldsymbol{x}})$ are the well-optimally concentrated Slepian functions in the region $\tilde{R}$, bandlimited to degree $L_{\tilde{g}} = 32$, a^j_β are random scalars drawn from the standard normal distribution and $N_{\tilde{R}} \approx 30$ is the rounded spherical Shannon number for the region $\tilde{R}$. The strength of these variations is specified by the background-to-variation ratio (BVR), defined as

$$\text{BVR} = 10\log\frac{\|b(\hat{\boldsymbol{x}})\|^2_{\mathbb{S}^2}}{\|v(\hat{\boldsymbol{x}})\|^2_{\mathbb{S}^2}}. \tag{56}$$

We generate $N = 10$ instances of the localized variations such that BVR is 20 dBs for each variation, yielding $N = 10$ different observations on the sphere as

$$f^j(\hat{\boldsymbol{x}}) = b(\hat{\boldsymbol{x}}) + \sum_{\beta=1}^{N_{\tilde{R}}\approx 30} a^j_\beta \tilde{g}_\beta(\hat{\boldsymbol{x}}), \qquad 1 \le j \le N = 10, \tag{57}$$

where each observation is bandlimited to degree $L_f = 32$. Magnitude of the source signal $b(\hat{\boldsymbol{x}})$ and the observation, which contains the first instance of localized variation, i.e., $f^1(\hat{\boldsymbol{x}})$, are shown in Fig. 7. As can be seen, the localized variation in the highlighted elliptical region is hidden in the source signal. It must be noted that the source signal, localized variations and the spherical elliptical region $\tilde{R}$ are unbeknownst to the framework of spatial-Slepian transform.

The presence of hidden variations is detected by obtaining the spatial-Slepian coefficients using the zonal Slepian functions for an axisymmetric north polar cap region R of polar cap angle $\Theta_c = 15°$, having bandlimit $L_g = 32$, and finding the sample variance across $N = 10$ different instances at each Slepian scale $\alpha = 1, \ldots N_{\Theta_c,0} = 3$. The results are shown in Fig. 8 where the unknown spherical elliptical region $\tilde{R}$ is drawn for reference only. For comparison, we also plot the sample variance of the scale-discretized wavelet coefficients,

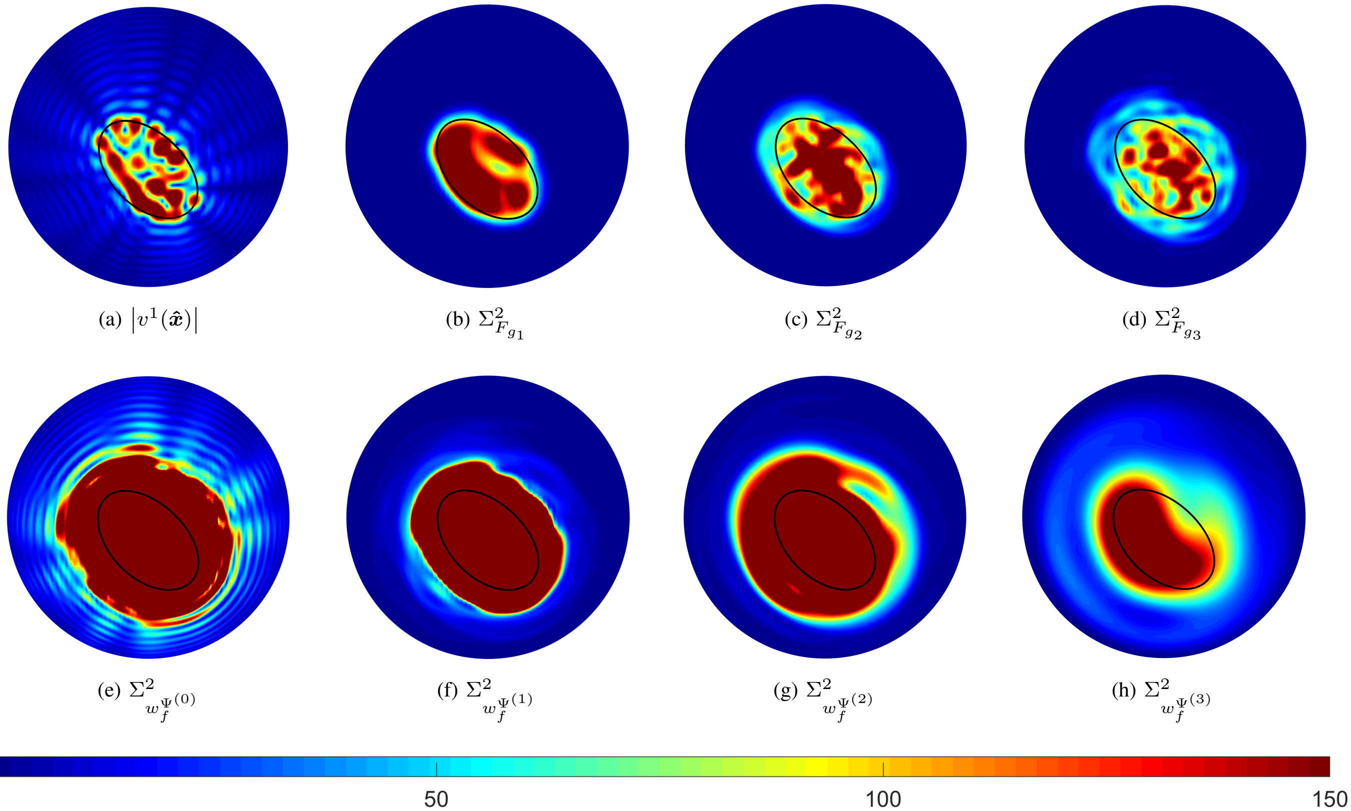

(a) $\left|v^1(\hat{\boldsymbol{x}})\right|$ (b) $\Sigma^2_{F_{g_1}}$ (c) $\Sigma^2_{F_{g_2}}$ (d) $\Sigma^2_{F_{g_3}}$

(e) $\Sigma^2_{w_f^{\Psi(0)}}$ (f) $\Sigma^2_{w_f^{\Psi(1)}}$ (g) $\Sigma^2_{w_f^{\Psi(2)}}$ (h) $\Sigma^2_{w_f^{\Psi(3)}}$

Fig. 8: (a) Magnitude of the first instance of localized variation, (b)–(d) sample variance of the spatial-Slepian coefficients $\Sigma^2_{F_{g_\alpha}}(\hat{\boldsymbol{y}}), \alpha = 1, \ldots, N_{\Theta_c,0} = 3$, $\hat{\boldsymbol{y}} \equiv \hat{\boldsymbol{y}}(\vartheta, \varphi)$, (e)–(h) sample variance of the scale-discretized wavelet coefficients $\Sigma^2_{w_f^{\Psi(s)}}(\hat{\boldsymbol{y}}), s = 0, 1, \ldots, 3$. As can be seen, sample variance of spatial-Slepian coefficients quite accurately detects the region of localized hidden variations at each Slepian scale, whereas sample variance of scale-discretized wavelet coefficients yields an over-estimate of the region of localized variations. The spherical elliptical region of localized hidden variations is unbeknownst to the framework of spatial-Slepian and scale-discretized wavelet transforms and is drawn for reference only.

which are obtained from the axisymmetric scale-discretized wavelet functions $\Psi^{(s)} \in L^2(\mathbb{S}^2)$ as [30]

$$w_f^{\Psi^{(s)}}(\hat{\boldsymbol{y}}) = \left\langle f, \left(\mathcal{D}_{\hat{\boldsymbol{y}}}\Psi^{(s)}\right)\right\rangle_{\mathbb{S}^2} = \int_{\mathbb{S}^2} f(\hat{\boldsymbol{x}})\overline{(\mathcal{D}_{\hat{\boldsymbol{y}}}\Psi^{(s)})(\hat{\boldsymbol{x}})}ds(\hat{\boldsymbol{x}}), \tag{58}$$

where $\hat{\boldsymbol{y}} \equiv \hat{\boldsymbol{y}}(\vartheta, \varphi)$ and s is the wavelet scale. Dilation parameter is set to 2, minimum wavelet scale is chosen to be 0, and maximum wavelet scale at bandlimit $L_f = 32$ is 5. However, we choose to show the sample variance for the first 4 wavelet scales as there is negligibly small sample variance at wavelet scales $s = 4, 5$.

As can be seen from Fig. 8, sample variance using the spatial-Slepian transform yields a very accurate detection of the hidden localized variations. In comparison, sample variance using the scale-discretized wavelet transform performs poorly; yielding an over-estimate of the underlying region of the localized variations. The superior performance of the spatial-Slepian transform is due to the fact that well-optimally concentrated Slepian functions are better suited to probe the local content of the signal than wavelet functions. Although wavelet functions have been shown to exhibit good spatial localization [30], unlike Slepian functions, their characteristics are not defined by the shape of the underlying region, which makes them ill-suited for localized signal analysis on the sphere.

VI. Conclusion

We have proposed spatial-Slepian transform (SST) for the representation of a spherical signal in the joint spatial-Slepian domain and for localized analysis of signals on the sphere. The proposed transform is similar in formulation to the scale-discretized wavelet transform, however, instead of using wavelet functions that cannot be adapted to a given region on the sphere, it uses bandlimited and spatially well-optimally (energy) concentrated Slepian functions, which enables it to probe the local contents of a signal. We have derived constraints under which the SST is invertible, presented an algorithm for the fast computation of spatial-Slepian coefficients, and carried out computational complexity analysis. We have numerically validated the proposed inverse SST using different realizations of a random test signal at various bandlimits. We have computed the spatial variance of spatial-Slepian coefficients and have conducted different experiments to show that spatial-Slepian coefficients have better spatial localization than scale-discretized wavelet coefficients. As an illustration, we have applied the proposed transform to a bandlimited Earth topography map using the zonal Slepian functions, which are well-optimally concentrated in the axisymmetric north polar cap region on the sphere. To demonstrate the utility of the proposed transform, we have also devised a framework to carry out localized variation analysis for the detection of hidden localized variations in the signal and have shown better performance of spatial-Slepian transform than scale-discretized wavelet transform in this regard. We consider the use of the proposed transform for carrying out localized signal analysis and optimal filtering as subjects of future work.

References

[1] S. Nadeem, Z. Su, W. Zeng, A. Kaufman, and X. Gu, "Spherical parameterization balancing angle and area distortions," *IEEE Transactions on Visualization and Computer Graphics*, vol. 23, no. 6, pp. 1663–1676, Jun. 2017.

[2] O. Michailovich and Y. Rathi, "On approximation of orientation distributions by means of spherical ridgelets," *IEEE Trans. Image Process.*, vol. 19, no. 2, pp. 461–477, Feb. 2010.

[3] A. P. Bates, Z. Khalid, and R. A. Kennedy, "An optimal dimensionality sampling scheme on the sphere with accurate and efficient spherical harmonic transform for diffusion MRI," *IEEE Signal Process. Lett.*, vol. 23, no. 1, pp. 15–19, Jan. 2016.

[4] L. C. C. Bergamasco, C. E. Rochitte, and F. L. S. Nunes, "3D medical objects processing and retrieval using spherical harmonics: a case study with congestive heart failure MRI exams," in *Proceedings of the 33rd Annual ACM Symposium on Applied Computing*. Pau, France: ACM, Apr. 2018, pp. 22–29.

[5] A. P. Bates, Z. Khalid, and R. A. Kennedy, "Novel sampling scheme on the sphere for head-related transfer function measurements," *IEEE/ACM Trans. Audio, Speech, Language Process.*, vol. 23, no. 6, pp. 1068–1081, Jun. 2015.

[6] H. Liu, Y. Fang, and Q. Huang, "Efficient representation of head-related transfer functions with combination of spherical harmonics and spherical wavelets," *IEEE Access*, vol. 7, pp. 78 214–78 222, Jun. 2019.

[7] T. Hoogenboom, S. E. Smrekar, F. S. Anderson, and G. Houseman, "Admittance survey of type 1 coronae on Venus," *J. Geophys. Res.*, vol. 109, no. 2, pp. 1–19, Mar. 2004.

[8] P. Audet, "Toward mapping the effective elastic thickness of planetary lithospheres from a spherical wavelet analysis of gravity and topography," *Physics of the Earth and Planetary Interiors*, vol. 226, pp. 48–82, Jan. 2014.

[9] M. Khaki, E. Forootan, M. Kuhn, J. Awange, L. Longuevergne, and Y. Wada, "Efficient basin scale filtering of GRACE satellite products," *Remote Sensing of Environment*, vol. 204, pp. 76–93, Jan. 2018.

[10] E. Galanti, Y. Kaspi, F. J. Simons, D. Durante, M. Parisi, and S. J. Bolton, "Determining the depth of Jupiter's great red spot with Juno: A Slepian approach," *The Astrophysical Journal Letters*, vol. 874, no. 2, Apr. 2019.

[11] M. v. Hippel and C. Harig, "Long-term and inter-annual mass changes in the Iceland ice cap determined from GRACE gravity using Slepian functions," *Cryospheric Sciences, Frontiers in Earth Science*, vol. 7, no. 171, Jul. 2019.

[12] M. A. Wieczorek and F. J. Simons, "Localized spectral analysis on the sphere," *Geophys. J. Int.*, vol. 162, no. 3, pp. 655–675, Sep. 2005.

[13] F. J. Simons and F. A. Dahlen, "Spherical Slepian functions and the polar gap in geodesy," *Geophys. J. Int.*, vol. 166, no. 3, pp. 1039–1061, Sep. 2006.

[14] F. A. Dahlen and F. J. Simons, "Spectral estimation on a sphere in geophysics and cosmology," *Geophys. J. Int.*, vol. 174, pp. 774–807, Sep. 2008.

[15] D. Marinucci, D. Pietrobon, A. Balbi, P. Baldi, P. Cabella, G. Kerkyacharian, P. Natoli, D. Picard, and N. Vittorio, "Spherical needlets for cosmic microwave background data analysis," *Monthly Notices Roy. Astron. Soc.*, vol. 383, no. 2, pp. 539–545, Jan. 2008.

[16] J. D. McEwen, S. M. Feeney, M. C. Johnson, and H. V. Peiris, "Optimal filters for detecting cosmic bubble collisions," *Phys. Rev. D.*, vol. 85, no. 10, p. 103502, May 2012.

[17] R. Grinter and G. A. Jones, "Interpreting angular momentum transfer between electromagnetic multipoles using vector spherical harmonics," *Optics letters*, vol. 43, no. 3, pp. 367–370, 2018.

[18] R. A. Kennedy, Z. Khalid, and Y. F. Alem, "Spatial correlation from multipath with 3D power distributions having rotational symmetry," in *Proc. IEEE Int. Conf. Sig. Process. and Comm. Sys., ICSPCS*, Carrara, VIC, Australia, Dec. 2013.

[19] Y. F. Alem, Z. Khalid, and R. A. Kennedy, "3D spatial fading correlation for uniform angle of arrival distribution," *IEEE Commun. Lett.*, vol. 19, no. 6, pp. 1073–1076, Jun. 2015.

[20] F. Bashar, T. D. Abhayapala, and S. M. A. Salehin, "Dimensionality of spatio-temporal broadband signals observed over finite spatial and temporal windows," *IEEE Transactions on Wireless Communications*, vol. 15, no. 10, pp. 6758–6770, Oct. 2016.

[21] R. Talashila and H. Ramachandran, "Determination of far fields of wire antennas on a PEC sphere using spherical harmonic expansion," *IEEE Antennas and Wireless Propagation Letters*, vol. 18, no. 4, pp. 646–650, Apr. 2019.

[22] S. G. Mallat, "A theory for multiresolution signal decomposition: the wavelet representation," *IEEE Trans. Pattern Anal. Mach. Intell.*, vol. 11, no. 7, pp. 674–693, Jul. 1989.

[23] I. Daubechies, "The wavelet transform, time-frequency localization and signal analysis," *IEEE Trans. Inf. Theory*, vol. 36, no. 5, pp. 961–1005, Sep. 1990.

[24] S. G. Mallat, *A Wavelet Tour of Signal Processing*, 3rd ed. Massachusetts, USA: Academic Press, 2009.

[25] F. J. Narcowich and J. D. Ward, "Non-stationary wavelets on the m-sphere for scattered data," *Appl. Comput. Harm. Anal.*, vol. 3, no. 4, pp. 324–336, Oct. 1996.

[26] F. Freeden and U. Windheuser, "Combined spherical harmonic and wavelet expansion – a future concept in the Earth's gravitational determination," *Appl. Comput. Harm. Anal.*, vol. 4, no. 1, pp. 1–37, Jan. 1997.

[27] J.-P. Antoine and P. Vandergheynst, "Wavelets on the 2-sphere: A group-theoretical approach," *Appl. Comput. Harm. Anal.*, vol. 7, no. 3, pp. 262–291, Nov. 1999.

[28] J.-L. Starck, Y. Moudden, P. Abrial, and M. Nguyen, "Wavelets, ridgelets and curvelets on the sphere," *Astron. & Astrophys.*, vol. 446, pp. 1191–1204, Feb. 2006.

[29] Y. Wiaux, J. D. McEwen, P. Vandergheynst, and O. Blanc, "Exact reconstruction with directional wavelets on the sphere," *Monthly Notices Roy. Astron. Soc.*, vol. 388, no. 2, pp. 770–788, Aug. 2008.

[30] J. D. McEwen, C. Durastanti, and Y. Wiaux, "Localisation of directional scale-discretised wavelets on the sphere," *Appl. Comput. Harm. Anal.*, vol. 44, no. 1, pp. 59–88, Jan. 2018.

[31] A. Albertella, F. Sansò, and N. Sneeuw, "Band-limited functions on a bounded spherical domain: the Slepian problem on the sphere," *J. Geodesy*, vol. 73, no. 9, pp. 436–447, Jun. 1999.

[32] F. J. Simons, F. A. Dahlen, and M. A. Wieczorek, "Spatiospectral concentration on a sphere," *SIAM Rev.*, vol. 48, no. 3, pp. 504–536, 2006.

[33] A. P. Bates, Z. Khalid, and R. A. Kennedy, "Slepian spatial-spectral concentration problem on the sphere: Analytical formulation for limited colatitude-longitude spatial region," *IEEE Trans. Signal Process.*, vol. 65, no. 6, pp. 1527–1537, Mar. 2017.

[34] ——, "Efficient computation of Slepian functions for arbitrary regions on the sphere," *IEEE Trans. Signal Process.*, vol. 65, no. 16, pp. 4379–4393, Aug. 2017.

[35] W. Nafees, Z. Khalid, and R. A. Kennedy, "Differential and weighted Slepian concentration problems on the sphere," *IEEE Trans. Signal Process.*, vol. 68, pp. 2830–2840, 2020.

[36] A. Aslam and Z. Khalid, "Localized analysis of signals on the sphere over polygon regions," *IEEE Trans. Signal Process.*, vol. 68, pp. 4568–4582, 2020.

[37] B. D. Wandelt and K. M. Górski, "Fast convolution on the sphere," *Phys. Rev. D.*, vol. 63, p. 123002, May 2001.

[38] R. A. Kennedy and P. Sadeghi, *Hilbert Space Methods in Signal Processing*. Cambridge, UK: Cambridge University Press, Mar. 2013.

[39] D. Slepian and H. O. Pollak, "Prolate spheroidal wave functions, Fourier analysis and uncertainity–I," *Bell Syst. Tech. J.*, vol. 40, no. 1, pp. 43–63, Jan. 1961.

[40] D. Slepian, "Prolate spheroidal wave functions, Fourier analysis and uncertainty–IV: Extensions to many dimensions; generalized prolate spheroidal functions," *Bell Syst. Tech. J.*, vol. 40, pp. 3009–3057, Nov. 1964.

[41] F. J. Simons and D. V. Wang, "Spatiospectral concentration in the cartesian plane," *Intern. J. Geo-math.*, vol. 2, no. 1, pp. 1–36, Apr. 2011.

[42] Z. Khalid, R. A. Kennedy, S. Durrani, P. Sadeghi, Y. Wiaux, and J. D. McEwen, "Fast directional spatially localized spherical harmonic transform," *IEEE Trans. Signal Process.*, vol. 61, no. 9, pp. 2192–2203, May 2013.

[43] J. D. McEwen, P. Vandergheynst, and Y. Wiaux, "On the computation of directional scale-discretized wavelet transforms on the sphere," in *Proc. Wavelets and Sparsity XV, SPIE international symposium on optics and photonics, invited contribution*, vol. 8858, San Diego, California, United States, Sep. 2013.

[44] S. Trapani and J. Navaza, "Calculation of spherical harmonics and Wigner *d* functions by FFT. Applications to fast rotational matching in molecular replacement and implementation into AMoRe," *Acta Cryst. A*, vol. 62, no. 4, pp. 262–269, Jul. 2006.

[45] T. Risbo, "Fourier transform summation of Legendre series and D-functions," *J. Geodesy*, vol. 70, no. 7, pp. 383–396, Jul. 1996.

[46] J. D. McEwen, M. P. Hobson, and A. N. Lasenby, "A directional continuous wavelet transform on the sphere," *Arxiv preprint astro-ph/0609159*, 2006.

Adeem Aslam (S'18) received his B.Sc. (with Honors) and M.Sc. degrees in Electrical Engineering from the University of Engineering and Technology Lahore, Pakistan, in 2009 and 2013 respectively. He has recently completed his Ph.D. in Electrical Engineering from the Lahore University of Management Sciences (LUMS), Lahore, Pakistan.

Adeem is currently working as an Assistant Professor in the department of Electrical Engineering, University of Engineering and Technology Lahore, Pakistan. During his Ph.D. studies, he was a recipient of a scholarship from the Higher Education Commission Pakistan, for indigenous PhD students, and a Syed Babar Ali Research Fellow at LUMS. His research interests include development of novel techniques for signal analysis on the sphere.

Zubair Khalid (S'10-M'13-SM'20) received his B.Sc. (First-class Hons.) degree in Electrical Engineering from the University of Engineering and Technology Lahore, Pakistan, in 2008. He received the Ph.D. degree in Engineering from the Australian National University of Canberra, Australia, in Aug. 2013.

He is currently working as an Assistant Professor in the department of Electrical Engineering, Lahore University of Management Sciences, Lahore, Pakistan. Zubair was awarded University Gold Medal and Industry Gold Medals from Siemens and Nespak for his overall outstanding performance in Electrical Engineering during his undergraduate studies. He was a recipient of an Endeavour International Postgraduate Award for his Ph.D. studies. His research interests are in the area of signal processing and wireless communication, including the development of novel signal processing techniques for signals on the sphere and application of stochastic geometry in wireless ad-hoc networks. Since 2020, he has been a member of the editorial board (Associate Editor) of IEEE Signal Processing Letters.